16th ICAAR LISBOA 2020-2022

16th International Conference on
Alkali-Aggregate Reaction in Concrete
Lisboa | LNEC | Portugal | 31 May - 2 June 2022

http://icaar2020-2022.lnec.pt

Calcium nitrate: A chemical admixture to inhibit aggregate dissolution and mitigate expansion caused by alkali-silica reaction

Tandré Oey [(1)], Erika Callagon La Plante [(2)], Gabriel Falzone [(2)], Yi-Hsuan Hsiao [(2)], Akira Wada [(2)], Linda Monfardini [(2)], Mathieu Bauchy [(2)], Jeffrey W. Bullard [(3)], Gaurav Sant [(2,4)]

(1) VTT Technical Research Centre, Espoo, Finland

(2) University of California, Los Angeles, CA, USA

(3) Texas A&M University, College Station, TX, USA

(4) Corresponding author: Gaurav Sant, gsant@ucla.edu

Abstract

Alkali-silica reaction (ASR) is a significant cause of degradation of concrete structures that results from the dissolution of reactive silicate aggregates and the associated formation of damaging, expansive ASR gels. Despite the prevalence of ASR, so far only lithium-based chemical admixtures have been successful in consistently mitigating its effects. Herein, it is demonstrated that dissolved calcium nitrate [$Ca(NO_3)_2$] can mitigate ASR-induced expansion, provoked using sodium borosilicate (NBS) glass as a model reactive aggregate. The ability of a highly soluble calcium salt to induce elevated concentrations of [Ca] species results in the rapid formation of surficial barrier films on dissolving aggregate surfaces that consist of calcium silicate hydrate (C-S-H) and/or calcite precipitates. The presence of such films hinders aggregate dissolution, resulting in a concurrent reduction in the rate of formation of expansion-inducing gels. The study highlights new, cost-effective, and presently unutilized pathways based on soluble alkaline-earth additives for suppressing ASR in concrete.

Keywords: *alkali-silica reaction; borosilicate glass; calcium nitrate; dissolution; expansion*

1. INTRODUCTION AND BACKGROUND

Formation of expansive gels by alkali-silica reaction (ASR) results in cracking and mechanical property degradations of concrete [1–3]. Due to ASR's damaging nature, and a diminishing supply of quality aggregates [4], reliable mitigation strategies are becoming increasingly important. Current approaches for mitigating ASR use silica-rich Class F fly ash and lithium-based admixtures [5–12]. These additives can effectively mitigate ASR damage, but they have several shortcomings including: (i) seasonal variations in the supply of Class F fly ash in the U.S. [13], (ii) heterogeneity and compositional variability of available fly ash compositions that result in different levels of ASR suppression from one fly ash to the other [14], and (iii) the prohibitively high cost of lithium-based admixtures [2]. As local supplies of non-reactive aggregates continue to dwindle, especially in urban areas, it may become necessary to utilize marginally reactive aggregates in concrete construction. However, this will only be possible if an effective, economical, reliable, and simple-to-implement approach is available for ASR mitigation.

Put simply, ASR occurs when reactive aggregates dissolve into the concrete's pore fluid, releasing silicon (Si) species at a rate or to an extent sufficient to precipitate hydrous alkali-silica gels [2]. The terminology "reactive aggregate" is somewhat ambiguous, so a quantitative metric is defined herein as the surface area-normalized dissolution rate of the aggregate. This choice reflects current understanding of ASR as a dissolution-precipitation process [2], whereby dissolved silicon forms Si-rich hydrate gels that cause expansion and damage. Aggregate dissolution is therefore a necessary first step of ASR, so suppressing the rate or extent of Si-dissolution would suppress the ASR process and its consequences. Based on this premise, and the noted ability of calcium to hinder silicate dissolution [15–17], this work demonstrates for the first time that calcium nitrate, an inexpensive and highly soluble calcium salt [18], inhibits both aggregate dissolution and mortar bar expansion concurrently. It is thereby able to mitigate ASR even when a highly reactive sodium borosilicate (NBS) glass is used as a model aggregate. Our observations suggest that calcium nitrate, and perhaps other alkaline earth salts, can form the basis for a novel, transformative, and cost-effective means of suppressing ASR in concrete systems.

2. MATERIALS AND METHODS

2.1 Materials and Specimen Preparation

An ASTM C150 compliant Type I/II ordinary portland cement (OPC) was used [19]. The cement's oxide equivalent composition measured by X-ray fluorescence (XRF) is reported in Table 2.1. Uncertainties reported represent the standard deviation of three replicate measurements. Alkali content expressed in Na_2O equivalent was 0.37%, consistent with a low-alkali OPC [19]. The mineralogical composition of the OPC determined by X-ray diffraction and Rietveld analysis is also reported in Table 2.1.

Table 2.1: The oxide equivalent and mineralogical compositions of the OPC used herein.

Oxide Phase	Composition (mass %)	Uncertainty (mass %)	Mineral Phase	Composition (mass %)	Uncertainty (mass %)
CaO	65.75	0.40	C_3S	57.8	1.60
SiO_2	20.54	0.40	C_2S	18.2	1.50
Al_2O_3	4.97	0.20	C_4AF	9.1	0.50
Fe_2O_3	3.10	0.10	C_3A	4.2	0.70
SO_3	2.75	0.10	$CaCO_3$	1.3	0.10
MgO	2.44	0.10	MgO	1.2	0.40
K_2O	0.29	0.01	$CaSO_4$	1.0	0.50
Na_2O	0.18	0.20	$CaSO_4 \cdot 0.5H_2O$	0.8	0.10
			$CaSO_4 \cdot 2H_2O$	0.5	0.20
			CaO	0.5	0.20

A recycled, crushed Type 33 alkali-borosilicate glass (NBS, Vitro Minerals [20]) was used as a model reactive siliceous aggregate, with a size gradation compliant with ASTM C441 [21, 22]. The oxide composition of the borosilicate glass as determined by SEM-EDS [23], was (81.4 ± 2.2) % SiO2, (12.0 ± 2.3) % B2O3, (4.7 ± 0.2) % Na2O, and (1.9 ± 0.2) % Al2O3, by mass. The specific surface area of the smallest glass sieve fraction specified by ASTM C441, sieve #50-100 (Table 2.2), is 27.7 ± 1.7 m^2/kg as measured by static light scattering (SLS, LS 13320, Beckman Coulter) performed on suspensions of the glass particles in isopropanol.

Table 2.2: The specific surface area and median particle diameter (d50) of the four size fractions of NBS glass particles, determined by static light scattering (SLS). The specific surface areas determined by this method have a coefficient of variation of about 5%.

Sample ID	Specific Surface Area (SSA, m^2/kg, from SLS)	d_{50} (μm)
Size 1 (Sieve #50-100)	27.7	76.4
Size 2	115	47.9
Size 3	210	15.9
Size 4	277	11.8

2.2 Experimental methods

2.2.1 Mortar bar expansion

The expansion of prismatic mortar bars (25 mm x 25 mm x 285 mm) was measured following a modified ASTM C441 protocol [21]. OPC and NBS glass (ASTM C441-compliant gradation) were mixed with deionized (DI) water to form mortars with water-cement mass ratio w/c = 0.50 following ASTM C305 [24]. The NBS glass particles, assumed to have a density of 2230 kg/m^3, were incorporated at volume

fractions of ϕ_a = 0.15, 0.25, 0.35, 0.45, and 0.55 of the total mortar volume. In select cases, the mortar bars also contained prescribed volume fractions of ASTM C778 compliant quartz sand with a density of 2650 kg/m^3. Three different calcium nitrate dosages, in addition to a control without calcium nitrate, were dissolved in the mixing water of mortars with ϕ_a = 0.25 NBS glass. These dosages were 1 mass %, 2 mass %, and 4 mass %, corresponding to 122 mmol/L, 244 mmol/L, and 488 mmol/L calcium nitrate.

Following casting, mortar bar specimens were cured for 24 hours under 100 % relative humidity (RH) at 25 ± 0.1 °C, 35 ± 0.1 °C, or 45 ± 0.1 °C. After 24 hours, specimens were removed from molds and cured for an additional 24 hours under 100 % RH at the same temperatures. After 48 hours from casting, the specimens were surface dried and the initial length was measured using a comparator [25]. The specimens were then cured under saturated (100 % RH) conditions at the same temperatures for either 200 days or until the length exceeded that which could be measured by the comparator. The length change was measured at intervals of 3 days to 14 days, from early to later ages. At least three replicate specimens were measured at each time and for each unique mortar bar formulation.

The rationale behind the above modifications of the ASTM C441 method was three-fold. First, the modifications enabled a quantitative comparison of the effects of reaction temperature on expansion. Second, it allowed the direct comparison of the effects of different aggregate volume fractions (ϕ_a) on expansion, including identification of a possible pessimum formulation [26]. Finally, the modifications made it possible to compare the influences of both temperature and ϕ_a with and without additions of calcium nitrate ($Ca(NO_3)_2$, abbreviated as CN where convenient). One benefit of this modified method is the ability to vary aggregate volume fractions and temperature to maximize the expansion. For example, a temperature of 45°C and aggregate volume fraction of ϕ_a = 0.25 produced the maximum amount of ASR-induced expansion. Consequently, these conditions were used determine how calcium nitrate performs in so-called a “worst case” ASR scenario.

2.2.2 Dissolution rate determination

To measure dissolution rate, 2.000 ± 0.005 g of NBS glass particles were added to 200 mL of a 10 mmol/L NaOH solution (pH 12) and sealed in high-density polyethylene (HDPE) bottles. While this solid-to-liquid ratio is in no way reflective of that between the aggregate and pore fluid in a realistic concrete, it provides a first point of comparison from which such an equivalence may be developed. Solutions were prepared by dissolving reagent grade NaOH in Milli-Q water (>18 MΩ·cm). The selection of the alkali cation, whether Na+ or K+, is expected to have little, if any, effect on the measured dissolution rates [3, 15]. Influence of dissolved salts on dissolution rate was tested by adding reagent grade calcium, aluminium, or lithium nitrate to the reference NaOH solution. The nitrate concentrations tested were (1, 10, 100, or 1000) mmol/L of $Ca(NO_3)_2$, (0.1, 0.5, or 1) mmol/L $Al(NO_3)_3$, and 1 mmol/L $LiNO_3$. Reference experiments were also performed for each of the four different particle sizes in Table 2.2.

The HDPE dissolution bottles were stored at 25 ± 0.1 °C, 35 ± 0.1 °C, or 45 ± 0.1 °C, and periodically agitated to limit particle settling, compaction, or cementation. The dissolution progress was measured by periodically withdrawing a small quantity of solution and measuring the concentrations of Si, Al, Ca, K, and Na by inductively-coupled-plasma optical emission spectrometry (ICP-OES). Specifically, 6 mL of the solution was withdrawn after 0, 1, 3, 6, 24, 72, and 168 hours, passed through a 0.2 µm syringe filter, and diluted by a factor of three with 5% (by volume) nitric acid (0.79 mmol/L HNO3) to stabilize the solution. Silicon and aluminium (axial view), as well as calcium, potassium, and sodium (radial view) were measured, with corresponding uncertainties of: ± 0.85 % for Si, ± 0.81 % for Al, ± 3.08 % for Ca, ± 1.35 % for K, and ± 6.15 % for Na (i.e., as determined by measurements carried out on a known reference solution). The composition data revealed a nearly linear increase in Si concentration with time for the first six hours, the slope of which was determined by linear regression, divided by the initial particle specific surface area, and used to characterize the initial dissolution rate in units of mmol/(m^2·s).

2.2.3 Surface analysis of NBS glass particles

Following 7 days of dissolution, the glass surfaces were vacuum-dried and characterized in terms of morphology, composition, and possible coverage by precipitates using scanning electron microscopy paired with energy dispersive spectroscopy (SEM-EDS, Phenom G2). SEM-EDS was conducted by mounting glass particles on copper tape and sputter-coating them with a few nanometres of gold prior to backscatter imaging (10 kV) and energy dispersive x-ray spectroscopy for elemental analysis (15 kV). Morphology and composition of the glass surfaces were assessed to detect surface precipitates. Sections extracted from the mortar samples were also prepared for SEM analysis, i.e., after 14 days of aging. These mortar fragments were subjected to solvent exchange in isopropanol to arrest hydration, after which they were stabilized in an epoxy resin and polished. These surfaces were also sputter-coated

with gold and analyzed in a manner identical to that described for the particles above, to assess compositional profiles in the near-surface region for the NBS glass particles.

2.2.4 Interrogation of other changes to the cementitious environment

To assess the influence of calcium nitrate additions on other aspects of the cementitious environment, measurements were made of the zeta potential of the glass particles, a proxy for surface charge (Zeta-PALS, Brookhaven Instruments Corporation). Suspensions of 0.01 % by mass of NBS glass particles of size 2 (Table 2.2) in a 10 mmol/L NaOH solution were prepared with and without calcium nitrate additions (see *Section 2.2.1*). The measurements were initiated within ≤ 10 minutes after adding the glass particles. A sequence of ten replicate measurements was acquired, with each measurement requiring about one minute to perform, from which the mean and standard deviation were calculated; no appreciable drift was observed across the ten measurements.

In addition to zeta potential measurements, the evolution of concentrations in the cement paste pore solution was measured. Cylindrical cement paste specimens were prepared for pore solution extractions at w/c = 0.45 according to ASTM C305, with 1 %, 2 %, or 4 % Ca(NO3)2 (by mass of cement) added to the mixing water. The specimens were stored at 25 °C and pore solutions were extracted at 1, 3, 7, and 28 days. Sodium, potassium, calcium, and aluminium concentrations in these solutions were measured by ICP-OES using the same extraction and dilution procedures as described in *Section 2.2.2*.

3. RESULTS AND DISCUSSION

3.1 Mortar expansion influenced by aggregate reactivity and volume fraction

The ASR-induced expansion strain of mortar bars, as shown in Figure 3.1(a), exhibits two distinct regimes: (1) an approximately linear increase, which gradually reaches (2) a plateau with little or no expansion, most evident at higher NBS volume fractions such as $\phi_a = 0.55$. A clearer comparison of the expansion kinetics for different ϕ_a is given in Figure 3.1(b) by normalizing the expansion strain by NBS volume fraction. This normalization causes the linear regimes in Figure 3.1(a) to collapse onto a single line at times up to 20 days, indicating that the initial rate of expansion is largely dictated by the availability of reactive NBS surface area (assumed proportional to volume fraction). Additionally, this normalization more clearly shows that the transition to a plateau happens at earlier times with increasing aggregate volume fraction.

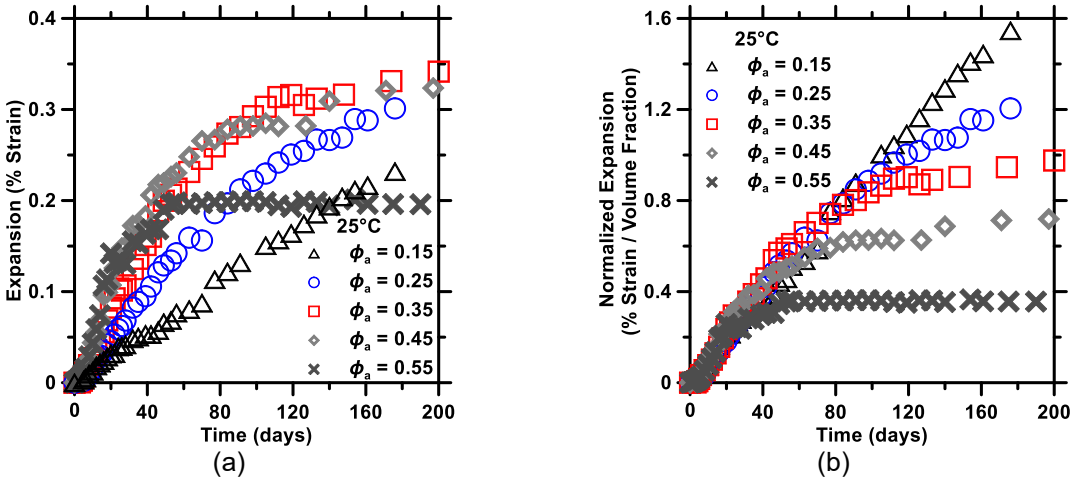

Figure 3.1: The (a) as-measured expansion, and (b) volume-fraction-normalized expansion of NBS glass-containing mortar bars at 25°C, for volume fractions, ϕ_a, ranging from 0.15 to 0.55.

Further quantitative analysis of the expansion behaviour was undertaken by parametrizing expansion profiles in terms of: (1) initial expansion rate, $R_{e,i}$, which is the initial slope of the curves in Figure 3.1(a) over the first 20 days; and (2) 200 day expansion, ε_{200}, i.e., the expansion measured after 200 days, an arbitrary choice to reflect a “mature” extent of expansion. Figure 3.2(a) shows the “mature” expansion at 200 days as a function of ϕ_a, suggesting a pessimum aggregate fraction (i.e., that for which the most expansion occurs), ϕ^*_a, of about 0.35 at 25 °C, or about 0.25 at 45 °C. That is, the strain at 200 days

increases with ϕ_a for $\phi_a < \phi^*_a$, but decreases at successively higher aggregate fractions. The behaviour below the pessimum is again consistent with the idea that ASR-induced expansion is proportional to the reactive aggregate surface area. However, the reverse trend when $\phi_a > \phi^*_a$ indicates that other factors besides reactive surface area likely affect the expansion at higher volume fractions.

To better understand the decrease in mature expansion strain (ε_{200}) with increasing ϕ_a for $\phi_a < \phi^*_a$, the NBS glass was partially replaced by inert quartz sand while leaving the total ϕ_a of aggregate unchanged. For example, the data shown as solid points in Figure 3.2 were obtained with ϕ_a = 0.55 = 0.15 NBS glass + 0.40 quartz sand. Replacing glass with quartz sand is expected to effectively reduce reactive surface area while leaving mortar stiffness broadly unchanged (N.B.: The NBS-glass and quartz sand feature stiffness values that are similar to each other, i.e., around 82 GPa for NBS-glass and 86 GPa for quartz, respectively [27, 28]). The early expansion rate of these quartz-substituted mortars (Figure 3.2(b)) was similar to that of their ϕ_a = 0.15 NBS glass-containing counterparts, though their expansion slowed more rapidly over time and reached a plateau similar to that of the ϕ_a = 0.55 NBS glass mortars (Figure 3.2(a)). This suggests that, while parameters such as the initial expansion rate ($R_{e,i}$) may better reflect the chemical effects of the aggregate (e.g., reactive surface area), the plateau behaviour and the mature extent of expansion (ε_{200}) are more strongly influenced by the mechanical stiffness. This is indicated by the reduction in expansion with increasing aggregate dosage beyond the pessimum, i.e., as the composite becomes stiffer, and appears to be insensitive to whether the aggregate is reactive (NBS) or not (quartz). Therefore, and to avoid the complexities of the pessimum effect and its variation with reaction temperature, here forward consideration will only be given to systems that feature an aggregate dosage at or below the pessimum (i.e., $\phi_a \leq 0.25$). This also justifies the reasons for using a modified ASTM C441 protocol, since the test method as formulated is implemented at 38°C and incorporates NBS glass at $\phi_a \approx 0.55$, i.e., in excess of the pessimum aggregate dosage for this material.

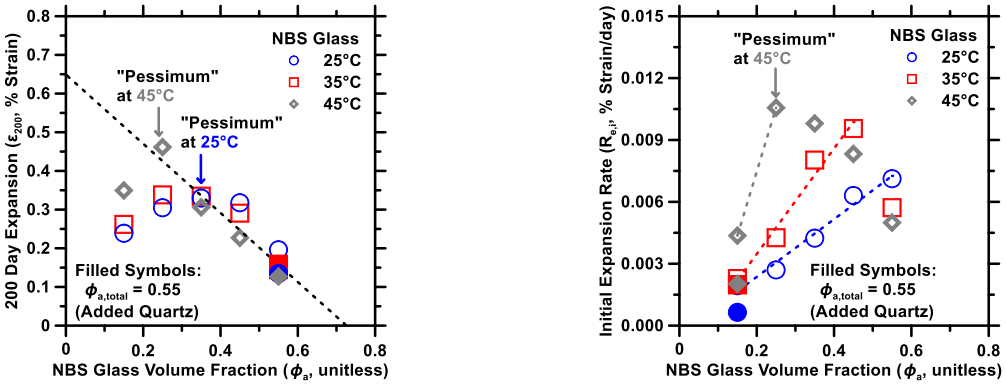

Figure 3.2: (a) The 200 d expansion data, ε200, plotted as a function of NBS glass volume fraction. A linear fit to strain for ϕa > ϕ*a is also shown. (b) The initial expansion rate of NBS glass mortar bars, Re,i, plotted as a function of the NBS glass volume fraction. The linear regressions suggest proportionality between ϕa and expansion rate for ϕa < ϕ*a. Data for quartz-substituted systems (ϕa,total = 0.55 = 0.15 NBS glass + 0.40 quartz sand) are shown as solid symbols for comparison.

Figure 3.3(a) compares how the initial expansion rates depend on temperature, ϕ_a, and calcium nitrate (CN) admixture dosage. The reference condition for this comparison is established at 45°C, ϕ_a = 0.25, and 0 % CN, which produces the highest rate and extent of expansion. As expected, the rate and extent of expansion is reduced by decreasing either the temperature or the aggregate volume fraction (i.e., surface area), or increasing the calcium nitrate dose. The effect of adding a modest amount of calcium nitrate (2 mass %) is to suppress the expansion rate similarly to either a 10 °C temperature reduction or a 10 % decrease in ϕ_a. Further increasing the dosage of CN produces even greater suppression of the expansion rate, more effective than even a 20 °C reduction in temperature. Figure 3.3(b) suggests that systems differing only in their CN dosage might converge to approximately equal expansion strain at late ages. That is, adding CN might only delay the ASR expansion and damage, by suppressing the initial reaction rates, rather than preventing ASR entirely. The efficacy of calcium nitrate in suppressing early-age ASR expansion rates may also possibly be caused by acceleration of early-age cement hydration and strength gain. However, this possibility can be rejected as CN's effect on increasing properties such as mortar stiffness and strength is effectively negligible for the dosages considered [29].

Even so, expansion data alone cannot conclusively reveal whether calcium nitrate acts by slowing the reaction rate per unit area or rather by reducing the total reactive surface area of the aggregates.

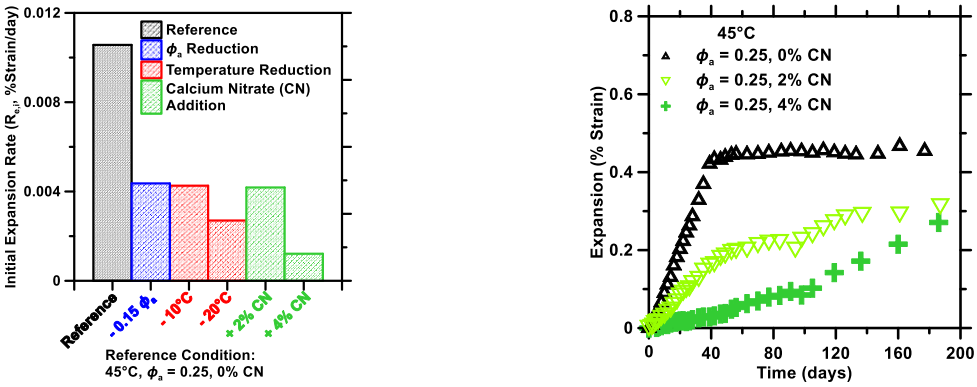

Figure 3.3: (a) A comparison between the initial expansion rates of cementitious mortar bars over the first 20 days for conditions encompassing: different NBS glass volume fractions (ϕa), reaction temperature, and calcium nitrate (CN) dosage. (b) A comparison between expansion profiles for the reference mortar bar and its Ca(NO3)2 containing counterparts, showing the progressive inhibition of expansion rate with increasing additive dosage.

3.2 Kinetics of dissolution of NBS glass in alkaline solutions

Since ASR is provoked by the presence of reactive aggregates [2], to offer a quantitative basis of discussion it is meaningful to assess the surface area-normalized reactivity of aggregates (i.e., NBS in the current case). This allows one to understand how the dosage of calcium nitrate ($Ca(NO_3)_2$, CN) affects dissolution rates, and in turn suppresses ASR-induced expansion.

Figure 3.4(a) shows representative silicon release profiles as a function of time at each temperature of interest in the absence of CN (in pH 12 NaOH). At early times < 6 hours, the concentration of solubilized silicon increased near-linearly, as typical for far-from-equilibrium dissolution [30–32]. After around 24 hours of dissolution, the silicon concentration in solution plateaued, as did the release of other elements (not shown). The plateau in dissolution for the reference system was not associated with the formation of precipitates nor saturation with respect to silicon (see *Section 3.4*). Aside from these two expected causes, an alternate explanation for the plateau may be the alteration of the NBS glass particle surfaces [33–37]. Despite the high pH, which is expected to limit the formation of altered layers on glass [37], SEM-EDS compositional profiles at NBS-glass particle surfaces confirmed the presence of Na- and Ca-enriched and Si-depleted regions (i.e., relative to the bulk NBS glass). While this provides an indication that the mechanisms controlling dissolution of Si change over time, specifics as to the stability and permeability of altered surface layers are lacking, requiring further work to elucidate how they may affect dissolution kinetics of glass, and other materials, in the context of ASR.

Significant reductions in dissolution rate are observed when either calcium (nitrate) or aluminium (nitrate) are present (Figure 3.4(b)), even at concentrations as low as 1 mmol/L [38]. Most mature concrete pore solutions contain similar concentrations of Ca and Al, suggesting that silicate glass dissolution may be inherently slower in cementitious environments, compared to that in pristine NaOH solutions (due to background abundance of Ca and Al resulting from OPC hydration). Calcium nitrate also produces a progressive reduction in dissolution rate with further increasing dosage (Figure 3.4(b)), up to about 100 mmol/L. For practical concrete applications such as set acceleration, CN is added to the mixing water at concentrations between 100 mmol/L and 500 mmol/L, so current usage of CN in industry, e.g., for set acceleration, is expected to be sufficient to achieve the dissolution suppression CN can likely provide.

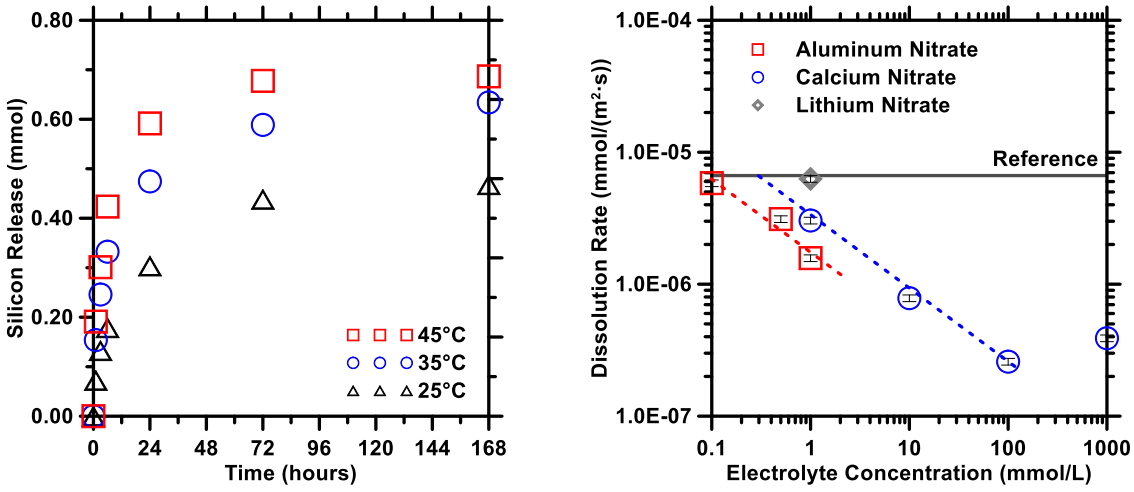

Figure 3.4: (a) Representative silicon release as a function of time and temperature, for the dissolution of NBS glass (Size 3, d50 = 15.9 μm) in a pH 12 (10 mmol/L NaOH) solution. (b) The dissolution rates of NBS glass (Size 3, d50 = 15.9 μm) in a pH 12 (10 mmol/L NaOH) solution dosed with Al, Ca, and Li nitrate salts, as a function of salt concentration.

3.3 Dissolution suppression by calcium goes beyond surface area reductions

The initial dissolution rates of the NBS glass are clearly seen to depend on temperature (Figure 3.4(a)). To quantify this temperature dependence, an effective activation energy of dissolution was calculated from the dissolution rates as a function of temperature:

$$r_d = r_{0,d} \exp\left(-E_{a,d}/RT\right) \quad (1)$$

where, $r_{0,d}$ is a pre-exponential factor (mmol/(m^2·s)), $E_{a,d}$ is the apparent activation energy of dissolution (J/mol), R is the gas constant (8.314 J/(mol·K)), and T is the temperature (K) [39].

This calculation produces an apparent activation energy of a reaction process comprising multiple dissolution steps such as network hydrolysis, surface diffusion, and bulk mass transport of dissolved species, without any distinctions made for these elementary reactions [30, 39, 40]. This apparent activation energy, which is expectedly similar for all size fractions of glass tested (those in Table 2.2), is $E_{a,d}$ = 32 ± 1.6 kJ/mol (Figure 3.5(a)). Although the dissolution rate of NBS glass should increase with pH in the basic regime, the effective activation energy should be pH-independent because nucleophilic attack of the silanol groups by OH- ions remains the dominant mechanism of dissolution [15, 30, 39]. Therefore, although the solution pH in which dissolution was evaluated, pH 12, is slightly lower than that of typical cementitious pore solutions [3], the activation energy is expected to be similar even as the pH increases. The reference effective activation energy is, however, expected to be lower than that applicable to NBS glass dissolution in realistic cementitious environments, in which low concentrations of calcium and aluminium present in the pore solution would reduce silicate dissolution rates [15–17, 41–44]. Activation energy increases substantially in the presence of even low concentrations of dissolved Ca or Al (Figure 3.5(a)). This implicates a fundamental change in the rate limiting step of dissolution by calcium, and not simply an effect related to a reduction in reactive surface area (e.g., by precipitate formation). It may suggest that this dissolution suppression by increases in activation energy, produced by low concentrations of either Ca or Al species, may be due to any of several effects, such as (1) their influence on near-surface transport of dissolved species [45]; (2) ion adsorption on reactive surface sites [41]; or (3) the formation of altered surface layers [16, 46].

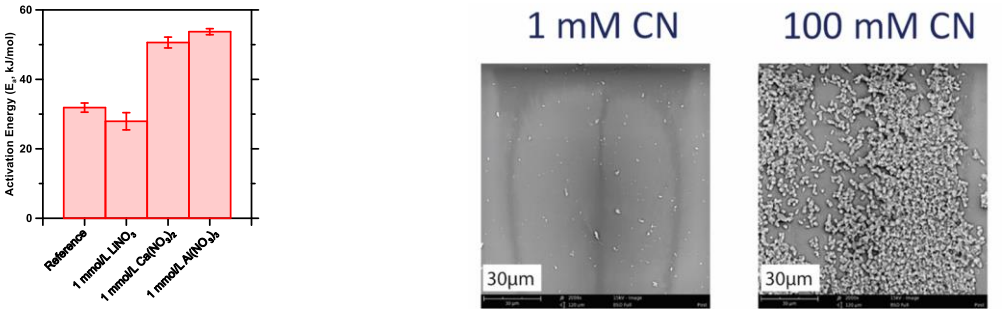

(a) (b)

Figure 3.5: (a) The activation energy (Ea, kJ/mol) of NBS glass dissolution in selected solution compositions from 25 °C ≤ T ≤ 45 °C, compared against the activation energy of mortar bar expansion over that same temperature range. (b) Representative SEM images of NBS glass surfaces exposed to pH 12 NaOH solutions for 7 days with 1 mmol/L or 100 mmol/L calcium nitrate. The surface coverage of precipitates forming on the NBS-glass surfaces increases dramatically with CN concentration, thus implicating the role of surficial barrier formation in dissolution inhibition. The image for 100 mmol/L CN has been republished with permission from (15).

Although the experiments performed here cannot distinguish the many individual elementary reactions that participate in ASR, it is still possible to link ASR-induced expansion with dissolution using apparent activation energy. Similar to the activation energy calculation discussed for the dissolution process, the temperature dependence of mortar bar expansion rates with NBS aggregate (*Section 3.1*) was also analysed using Equation 1 to obtain an apparent activation energy expansion of about 50 kJ/mol. This value is quite close to the activation energy of dissolution of NBS in the presence of low concentrations of calcium or aluminium, i.e., that expected to dictate aggregate reactivity in most mature cementitious systems (e.g., Figure 3.6(a)), which is also about 50 kJ/mol (Figure 3.5(a)). The near-equality of the two activation energies therefore is either a surprising coincidence or, more likely, indirect evidence that the rate of the dissolution process largely controls the overall rate of ASR-induced expansion. The beneficial effects conveyed by calcium nitrate, therefore, are likely not observed in typical OPC-based systems because the initial Ca-concentrations in those systems are not high enough to induce the formation of the surface precipitates (Figure 3.5(b)), which appear to be pre-requisite to reducing reactive surface area and thereby suppressing the silicate dissolution rate sufficiently to mitigate ASR.

3.4 Surface barriers form rapidly but require higher Ca concentrations

Despite the expected changes to silicate dissolution mechanism induced by the presence of calcium, geochemical analysis of the solution composition data over the course of dissolution, i.e., using PHREEQC [47, 48] and GEMS [49, 50], reveals that when CN is added at concentrations in excess of 10 mmol/L the solution rapidly (≤ 1 h) becomes supersaturated with respect to calcite and calcium silicate hydrate (C-S-H) for pH > 12, with the latter expected to precipitate in larger amounts. In light of this, the influence on glass dissolution of calcium nitrate and similar alkaline earth salts is likely associated with two factors. The first, already touched upon earlier, is the interactions of calcium ions with the glass surface [16], which increases the effective activation energy of the dissolution process. However, the supersaturation of the solution with respect to calcite and C-S-H for higher concentrations suggests that a second and concurrent effect is the formation of calcium-bearing precipitates on reacting particle surfaces [15–17], which can form a diffusion barrier and partially passivate the surface by reducing its exposed reactive area. Realistic cementitious systems have solutions that evolve in composition over time, especially at early times before the solution approaches equilibrium with respect to the precipitated solids. In those systems, additives such as calcium nitrate can increase the calcium concentration at early ages, but at later ages the calcium concentration will still be effectively constrained by chemical equilibrium considerations, as suggested by the pore solution data shown in Figure 3.6(a).

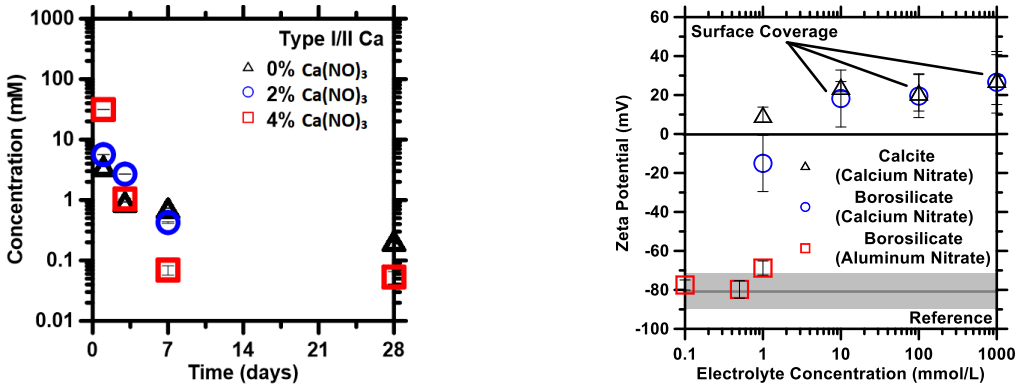

(a) (b)

Figure 3.6: (a) The concentration of Ca-species in extracted cementitious pore solution as a function of time for both Ca(NO3)2-dosed and calcium nitrate free systems, and (b) The zeta potential of calcite and NBS-glass particles in contact with pH 12 (10 mmol/L NaOH) solutions containing different concentrations of calcium (and aluminium) nitrate. The shaded grey region shows the zeta potential that is measured under additive-free conditions (the width of the grey region shows the standard deviation of replicate measurements).

Therefore, the dissolution and expansion suppression produced by calcium nitrate is expected to be caused primarily by the early formation of stable, calcium-containing precipitates on the glass surfaces which then persist on those surfaces over time. The rapid, early formation of such precipitate films, as directly observed by SEM-EDS analysis following dissolution experiments (Figure 3.5(b)), was also confirmed by measuring zeta potential. Zeta potential is the electric potential at the shear boundary between static and flowing solution at the surface of moving particles, which is used here as a proxy for particle surface charge. Figure 3.6(b) indicates significant changes in zeta potential upon addition of calcium nitrate additive, suggesting precipitation of calcite on their surfaces. All the zeta potential measurements were made within the first 10 minutes after introducing the particles to the solution, indicating that surface precipitates form relatively quickly, consistent with geochemical analyses.

4. SUMMARY AND CONCLUSIONS

Using a highly reactive sodium borosilicate (NBS) glass as a model ASR-reactive aggregate, this study has shown, for the first time, that calcium nitrate additions effectively inhibit aggregate dissolution and, in turn, mortar bar expansion. These processes are shown to be closely related, as highlighted by their nearly identical apparent activation energies. This suggests that the aggregate dissolution process dictates the progress of ASR. Furthermore, this work suggests that any chemical additive capable of inhibiting reactive silicate dissolution, i.e., regardless of its operating mechanism, can serve as a viable ASR mitigation method. For example, high dosages of soluble alkaline-earth salts could promote the precipitation of C-S-H or calcite to partially cover and passivate the dissolving aggregate surface, as shown herein. ASR inhibitors could also in the future be quantitatively evaluated by measuring their influence on aggregate dissolution rates, although this would require the development of a cost-effective standard test method for such measurement. This work also highlights the need for further study of how surface alterations affect chemical reaction rates, which is important to distinguish how intrinsic reactivity reductions versus physical coverage are important in affecting ASR reaction rates. Surface reactivity changes are indeed important, as suggested in this study, but physical surface coverage is perhaps even more important for reducing the rate and extent of aggregate dissolution during ASR. This latter aspect especially dictates why ASR mitigation can be achieved by the use of soluble alkaline-earth salts.

5. ACKNOWLEDGEMENTS

The authors acknowledge financial support for this research provisioned by COMAX: a joint UCLA-NIST consortium that is supported by industry and government agency partners, the Department of Energy's Nuclear Energy University Program (DE-NE0008398), and the National Science Foundation (CAREER Award: 1253269). The contents of this paper reflect the views and opinions of the authors, who are responsible for the accuracy of data presented herein. This research was conducted in the Laboratory

for the Chemistry of Construction Materials (LC2) and the Molecular Instrumentation Center (MIC) at the University of California, Los Angeles (UCLA). The authors gratefully acknowledge the support that has made these laboratories and their operations possible. GNS acknowledges discretionary support for this research provided by the Henry Samueli Fellowship, and many years of insightful discussions with Prof. Jacob N. Israelachvili (UC-Santa Barbara) on the mechanisms of silicate dissolution.

6. REFERENCES

[1] Lamond J, Pielert J (2006) Significance of tests and properties of concrete and concrete-making materials. ASTM, West Conshohocken.

[2] Rajabipour F, Giannini E, Dunant C, et al (2015) Alkali–silica reaction: Current understanding of the reaction mechanisms and the knowledge gaps. Cem Concr Res 76:130–146. https://doi.org/10.1016/j.cemconres.2015.05.024

[3] Swamy R (2002) The alkali-silica reaction in concrete. CRC Press, Boca Raton.

[4] Miller R, Bush L (2014) Update of Mineral Land Classification for Portland Cement Concrete Grade Aggregate in the Temescal Valley Production Area, Riverside County. Report No. 231.

[5] McCoy WJ, Caldwell AG (1951) New approach to inhibiting alkali-aggregate expansion. J Proc 47:693-706.

[6] Thomas M (2011) The effect of supplementary cementing materials on alkali-silica reaction: A review. Cem Concr Res 41:1224–1231. https://doi.org/10.1016/j.cemconres.2010.11.003

[7] Mahyar M, Erdoğan S (2018) Extension of the chemical index model for estimating Alkali-Silica reaction mitigation efficiency to slags and natural pozzolans. Constr Build Mater 179:587-597.

[8] Kim T, Olek J (2016) The effects of lithium ions on chemical sequence of alkali-silica reaction. Cem Concr Res 79:159-168.

[9] Tremblay C, Berube M, Fournier B, Thomas M (2004) Performance of lithium-based products against ASR: effect of aggregate type and reactivity, and reaction mechanisms. Proc Seventh CANMET/ACI Internati Conf Recent Adv Concr Technol 247–267.

[10] Tremblay C, Bérubé MA, Fournier B, Thomas MD, Folliard K (2007) Effectiveness of lithium-based products in concrete made with Canadian natural aggregates susceptible to alkali-silica reactivity. ACI Mater J 104:195.

[11] Drimalas T, Ideker J, Bentivegna AF, Folliard KJ, Fournier B, Thomas MD (2012) The Long-Term Monitoring of Large-Scale Concrete Specimens Containing Lithium Salts to Mitigate Alkali-Silica Reaction. Spec Pub 289:1-17.

[12] Ekolu S, Rakgosi G, Hooton D (2017) Long-term mitigating effect of lithium nitrate on delayed ettringite formation and ASR in concrete–Microscopic analysis. Mater Charact 133:165-175.

[13] Rea C, Darby K, Suszko C, et al (2016) Fly Ash: Current and Future Supply.

[14] Oey T, Timmons J, Stutzman P, Bullard JW, Balonis M, Bauchy M, Sant G (2017) An improved basis for characterizing the suitability of fly ash as a cement replacement agent. J Am Ceram Soc 100:4785–4800. https://doi.org/10.1111/jace.14974

[15] La Plante EC, Oey T, Hsiao Y-H, Perry L, Bullard JW, Sant G (2019) Enhancing Silicate Dissolution Kinetics in Hyperalkaline Environments. J Phys Chem C 123:3687–3695. https://doi.org/10.1021/acs.jpcc.8b12076

[16] Mercado-Depierre S, Angeli F, Frizon F, Gin S (2013) Antagonist effects of calcium on borosilicate glass alteration. J Nucl Mater 441:402-410.

[17] Maraghechi H, Rajabipour F, Pantano CG, Burgos W (2016) Effect of calcium on dissolution and precipitation reactions of amorphous silica at high alkalinity. Cem Concr Res 87:1-13.

[18] Calcium Nitrate: Compound Summary. https://pubchem.ncbi.nlm.nih.gov/compound/Calcium-nitrate. Accessed 2 January 2020.

[19] (2016) ASTM Standard C150/C150M-16e1 Standard Specification for Portland Cement.

[20] Vitro Minerals. http://www.vitrominerals.com/order-samples/c-441-test-grade/

[21] (2011) ASTM Standard C441/C441M-11 Standard Test Method for Effectiveness of Pozzolans or Ground Blast-Furnace Slag in Preventing Excessive Expansion of Concrete Due to the Alkali-Silica Reaction.

[22] (2014) ASTM Standard C1260-14 Standard Test Method for Potential Alkali Reactivity of Aggregates (Mortar-Bar Method).

[23] Stutzman P, Feng P, Bullard JW (2016) Phase analysis of Portland cement by combined quantitative X-ray powder diffraction and scanning electron microscopy. J Res Nati Inst Stand Technol 121:47-107.

[24] (2014) ASTM Standard C305-14 Standard Practice for Mechanical Mixing of Hydraulic Cement Pastes and Mortars of Plastic Consistency.

[25] (2011) ASTM C490/490M-11e1 Standard Practice for Use of Apparatus for the Determination of Length Change of Hardened Cement Paste, Mortar, and Concrete.

[26] Binal A (2015) The pessimum ratio and aggregate size effects on alkali silica reaction. Proc Earth Planetary Sci 15:725-731.

[27] Spinner SAM (1956) Elastic Moduli of Glasses at Elevated Temperatures by a Dynamic Method. J Am Ceram Soc 39:113–118. https://doi.org/10.1111/j.1151-2916.1956.tb15634.x

[28] McSkimin HJ, Andreatch P, Thurston RN (1965) Elastic Moduli of Quartz versus Hydrostatic Pressure at 25° and − 195.8°C. J Appl Phys 36:1624–1632. https://doi.org/10.1063/1.1703099

[29] Oey T, Stoian J, Li J, Vong C, Balonis M, Kumar A, Franke W, Sant G (2015) Comparison of Ca(NO3)2 and CaCl2 Admixtures on Reaction, Setting, and Strength Evolutions in Plain and Blended Cementing Formulations. J Mater Civ Eng 27:04014267. https://doi.org/10.1061/(ASCE)MT.1943-5533.0001240

[30] Brantley SL (2008) Kinetics of Mineral Dissolution. In: Kinetics of Water-Rock Interaction. Springer, New York.

[31] Lüttge A (2006) Crystal dissolution kinetics and Gibbs free energy. J Electron Spectros Relat Phenomena 150:248–259. https://doi.org/10.1016/j.elspec.2005.06.007

[32] Arvidson RS, Luttge A (2010) Mineral dissolution kinetics as a function of distance from equilibrium–New experimental results. Chem Geol 269:79-88.

[33] Cailleteau C, Devreux F, Spalla O, Angeli F, Gin S (2011) Why Do Certain Glasses with a High Dissolution Rate Undergo a Low Degree of Corrosion? J Phys Chem C 115:5846–5855. https://doi.org/10.1021/jp111458f

[34] Cailleteau C, Angeli F, Devreux F, Gin S, Jestin J, Jollivet P, Spalla O (2008) Insight into silicate-glass corrosion mechanisms. Nat Mater 7:978.

[35] Hellmann R, Cotte S, Cadel E, Malladi S, Karlsson LS, Lozano-Perez S, Cabié M, Seyeux A (2015) Nanometre-scale evidence for interfacial dissolution–reprecipitation control of silicate glass corrosion. Nat Mater 14:307.

[36] Hellmann R, Wirth R, Daval D, Barnes JP, Penisson JM, Tisserand D, Epicier T, Florin B, Hervig RL (2012) Unifying natural and laboratory chemical weathering with interfacial dissolution–reprecipitation: a study based on the nanometer-scale chemistry of fluid–silicate interfaces. Chem Geol 294:203-216.

[37] Hamilton JP, Patano CG (1997) Effects of glass structure on the corrosion behavior of sodium-aluminosilicate glasses. J Non Cryst Solids 222:167-174.

[38] Lothenbach B, Winnefeld F, Alder C, Wieland E, Lunk P (2007) Effect of temperature on the pore solution, microstructure and hydration products of Portland cement pastes. Cem Concr Res 37:483-491.

[39] Icenhower JP, McGrail BP, Shaw WJ, Pierce EM, Nachimuthu P, Shuh DK, Rodriguez EA, Steele JL (2008) Experimentally determined dissolution kinetics of Na-rich borosilicate glass at far from equilibrium conditions: implications for transition state theory. Geochimica Cosmochimica Acta 2767-2788.

[40] Icenhower JP, Steefel CI (2013) Experimentally determined dissolution kinetics of SON68 glass at 90 Cover a silica saturation interval: Evidence against a linear rate law. J Nucl Mater 439:137-147.

[41] Bickmore BR, Nagy KL, Gray AK, Brinkerhoff AR (2006) The effect of Al (OH) 4− on the dissolution rate of quartz. Geochimica Cosmochimica Acta 70:290-305.

[42] Chappex T, Scrivener KL (2012) The Effect of Aluminum in Solution on the Dissolution of Amorphous Silica and its Relation to Cementitious Systems. J Am Ceram Soc 96:592-597 https://doi.org/10.1111/jace.12098

[43] Houston JR, Herberg JL, Maxwell RS, Carroll SA (2008) Association of dissolved aluminum with silica: Connecting molecular structure to surface reactivity using NMR. Geochimica Cosmochimica Acta 72:3326-3337.

[44] Mason HE, Maxwell RS, Carroll SA (2011) The formation of metastable aluminosilicates in the Al–Si–H2O system: Results from solution chemistry and solid-state NMR spectroscopy. Geochimica Cosmochimica Acta 75:6080-6093.

[45] Brantley SL (2003) Reaction Kinetics of Primary Rock-forming Minerals under Ambient Conditions. In: Treatise on Geochemistry 73–117. Ed. RW Carlson, Amsterdam.

[46] Angeli F, Boscarino D, Gin S, Della Mea G, Boizot G, Petit JC (2001) Influence of calcium on sodium aluminosilicate glass leaching behaviour. Phys Chem Glasses 42:279-286.

[47] Parkhurst D, Appelo C (2013) Description of input and examples for PHREEQC version 3: a computer program for speciation, batch-reaction, one-dimensional transport, and inverse geochemical calculations. USGS, Reston.

[48] Charlton SR, Parkhurst DL, (2011) Modules based on the geochemical model PHREEQC for use in scripting and programming languages. Computers Geosci 37:1653-1663.

[49] Wagner T, Kulik DA, Hingerl FF, Dmytrieva SV (2012) GEM-Selektor geochemical modeling package: TSolMod library and data interface for multicomponent phase models. Canadian Mineralogist 50:1173-1195.

[50] Kulik DA, Wagner T, Dmytrieva SV, Kosakowski G, Hingerl FF, Chudnenko KV, Berner UR (2013) GEM-Selektor geochemical modeling package: revised algorithm and GEMS3K numerical kernel for coupled simulation codes. Computational Geosci 17:1-24.